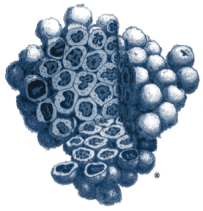

STEM CELLS®

Magnetic Resonance-Based Tracking and Quantification of Intravenously Injected Neural Stem Cell Accumulation in the Brains of Mice with Experimental Multiple Sclerosis

Letterio S. Politi, Marco Bacigaluppi, Elena Brambilla, Marcello Cadioli, Andrea Falini, Giancarlo Comi, Giuseppe Scotti, Gianvito Martino and Stefano Pluchino

Stem Cells 2007;25;2583-2592; originally published online Jun 28, 2007;
DOI: 10.1634/stemcells.2007-0037

STEM CELLS®

TECHNOLOGY DEVELOPMENT

Magnetic Resonance-Based Tracking and Quantification of Intravenously Injected Neural Stem Cell Accumulation in the Brains of Mice with Experimental Multiple Sclerosis

LETTERIO S. POLITI,[a,b] MARCO BACIGALUPPI,[c,d,e] ELENA BRAMBILLA,[c,d] MARCELLO CADIOLI,[b,f] ANDREA FALINI,[a,b] GIANCARLO COMI,[d,e] GIUSEPPE SCOTTI,[a,b] GIANVITO MARTINO,[c,d,e] STEFANO PLUCHINO[c,d]

[a]Neuroradiology Unit, [b]Centro Eccellenza Risonanza Magnetica ad Alto Campo, [c]Neuroimmunology Unit, Department of Biological and Technological Research (DIBIT), [d]Institute of Experimental Neurology (InSpe), [e]Department of Neurology and Neurophysiology, San Raffaele Scientific Institute, Milan, Italy; [f]Philips Medical Systems, Eindhoven, The Netherlands

Key Words. Transplantation • Neural stem cells • Multiple sclerosis • Magnetic resonance imaging • Superparamagnetic iron oxide

ABSTRACT

Eliciting the in situ accumulation and persistence patterns of stem cells following transplantation would provide critical insight toward human translation of stem cell-based therapies. To this end, we have developed a strategy to track neural stem/precursor cells (NPCs) in vivo using magnetic resonance (MR) imaging. Initially, we evaluated three different human-grade superparamagnetic iron oxide particles for labeling NPCs and found the optimal labeling to be achieved with Resovist. Next, we carried out in vivo experiments to monitor the accumulation of Resovist-labeled NPCs following i.v. injection in mice with experimental autoimmune encephalomyelitis (EAE), the animal model of multiple sclerosis. With a human MR scanner, we were able to visualize transplanted cells as early as 24 hours post-transplantation in up to 80% of the brain demyelinating lesions. Interestingly, continued monitoring of transplanted mice indicated that labeled NPCs were still present 20 days postinjection. Neuropathological analysis confirmed the presence of transplanted NPCs exclusively in inflammatory demyelinating lesions and not in normal-appearing brain areas. Quantification of transplanted cells by means of MR-based ex vivo relaxometry (R2*) showed significantly higher R2* values in focal inflammatory brain lesions from EAE mice transplanted with labeled NPCs as compared with controls. Indeed, sensitive quantification of low numbers of NPCs accumulating into brain inflammatory lesions (33.3–164.4 cells per lesion; $r^2 = .998$) was also obtained. These studies provide evidence that clinical-grade human MR can be used for noninvasive monitoring and quantification of NPC accumulation in the central nervous system upon systemic cell injection. STEM CELLS *2007;25:2583–2592*

Disclosure of potential conflicts of interest is found at the end of this article.

INTRODUCTION

Preclinical evidence indicates that transplantation of neural stem/precursor cells (NPCs) has a definite therapeutic relevance in chronic central nervous system (CNS) disorders characterized by either inflammation or degeneration [1]. Whatever the mechanism(s) underlying the therapeutic efficacy—either cell replacement or bystander immunomodulation, a key issue to address for translation into the clinic is the development of an in vivo, noninvasive method for tracking the transplanted cells.

Nuclear medicine techniques, fluorescence imaging, and bioluminescence are noninvasive imaging approaches that have been shown to provide valuable means for monitoring cell therapies in vivo. Positron emission tomography has been used in humans to evaluate viability and function of locally transplanted cells in the neurodegenerative disorders Parkinson and Huntington diseases [2, 3]. Fluorescence imaging and bioluminescence have been successfully used to monitor focal stem cell transplantation in mice with cerebral infarcts [4]. Unfortunately, all these techniques show poor spatial resolution, cannot be correlated to anatomical details, and have limited depth penetration [5].

In contrast to these latter techniques, magnetic resonance (MR) imaging is a more accurate means for cellular imaging [6], which allows efficacious tracking over longer periods of time. According to the data collected so far, MR imaging possesses remarkable resolution, allows direct anatomic correlation on the same image, and can be performed and repeated several times on living subjects [7].

The recent development of superparamagnetic iron oxides (SPIOs) has further improved the sensitivity of cellular and molecular MR imaging [8]. Magnetically labeled oligodendrocyte progenitors [9, 10], neural progenitors [11, 12], and Schwann cells [13] focally transplanted into preclinical rodent models of genetic or focal chemical demyelination/dysmyelination have been visualized with high magnetic field strength animal-dedicated MR scanners. More recently, proof-of-principle studies have reported that detection of iron-labeled trans-

Correspondence: Stefano Pluchino, M.D., Ph.D., Neuroimmunology Unit, Department of Biological and Technological Research (DIBIT)-San Raffaele Scientific Institute, Via Olgettina 58, 20123 Milan, Italy. Telephone: +39 02 26432791; Fax: +39 02 26434855; e-mail: pluchino.stefano@hsr.it Received January 15, 2007; accepted for publication June 17, 2007; first published online in STEM CELLS *EXPRESS* June 28, 2007. 1066-5099/2007/$30.00/0 doi: 10.1634/stemcells.2007-0037

planted somatic (stem) cells in bodily organs other than the CNS can be obtained by human-grade MR [6, 14, 15]. Moreover, using this approach, quantification can be achieved by means of T_2* relaxometry [16]. However, clinical-grade MR imaging has still not been proven to be sensitive enough to detect and quantify low numbers of transplanted cells in situ [16].

In this study, we demonstrate the feasibility of noninvasive clinical-grade quantitative MR imaging of systemically injected tissue-specific adult stem cells. Using a mouse model of chronic multiple sclerosis (MS), we show that sensitive detection of intravenously injected SPIO-labeled NPCs can be achieved by clinical-grade MR imaging and subsequent quantification by ex vivo relaxometry. This enabled us to determine that systemic delivery of NPCs results in small numbers of transplanted NPCs (down to 30 cells per site) accumulating within focal inflammatory demyelinating brain lesions. These findings validate the advantage of using noninvasive MR imaging for monitoring NPC-based therapies and represent a significant step toward the design of future clinical trials for somatic stem cell transplantation in MS.

Materials and Methods

NPC Derivation and Cultures

NPC cultures were established from the subventricular zone of 3-month-old C57BL/6 mice as previously described [17, 18]. Further information is provided in the supplemental online Methods.

NPC Labeling with SPIOs

Endorem, 80–150 nm (AMI-25; Guerbet, Paris, http://www.guerbet.com), Food and Drug Administration (FDA)-approved, Resovist, 62 nm (SHU-555A; Schering, Berlin, http://www.schering.de), FDA-approved, and Sinerem, 20–40 nm (AMI-277; Guerbet), phase III clinical-trial completed [19], were compared. Further information is provided in the supplemental online Methods.

Perl's Prussian Blue Staining

Single-cell-dissociated SPIO-labeled NPCs plated onto Matrigel-coated glass coverslips or cryo-tissue sections were washed in 1× phosphate-buffered saline (PBS) (without Ca^{2+} and Mg^{+}) to remove the excess of contrast agent and were fixed for 5 minutes with 4% paraformaldehyde (Sigma-Aldrich, St. Louis, http://www.sigmaaldrich.com). Prussian blue (PB) staining was performed by incubation in a 1:1 mixture of 6% HCl (AnalaR; BDH Laboratory Supplies, Poole, Dorset, U.K.) and 2% potassium ferrocyanide (Sigma) for 30 minutes at room temperature (24°C). A minimum of $n \geq 8$ nonoverlapping fields was counted for each sample. Nuclei were counterstained by nuclear red. Data were expressed as mean percentage of PB-positive cells (over total of plated cells as determined by nuclear staining) ± SEM calculated from a total of $n \geq 3$ independent experiments.

Electron Microscopy

Resovist-labeled NPCs were extensively washed, fixed with 4% glutaraldehyde for 30 minutes, postfixed in osmium tetroxide for 1 hour, dehydrated in ascending alcohol concentrations, and embedded in TAAB resin (TAAB Laboratories, Aldermaston, U.K., http://www.taab.co.uk). Ultrathin sections were mounted onto slot grids for viewing using a Hitachi H600 transmission electron microscope (Hitachi, Tokyo, http://www.hitachi.com) as previously described [18].

In Vitro MR Imaging

For gelatin phantom experiments, NPCs were labeled with 0.1 mg/ml Resovist, washed with PBS (without Ca^{2+} and Mg^{+}), and then resuspended in 5 μl of 4% low-melting agarose (Sigma) at 56°C containing 10^4, 10^3, 10^2, or 10 cells. The cell-containing agarose suspension was then transferred into a 4% low-melt agarose preloaded 48-well plate and processed for MR imaging using sequences and protocols described below. In vitro MR studies were performed using a 1.5T human MR scanner (Intera 1.5T; Philips Medical Systems, Andover, MA, http://www.medical.philips.com) equipped with 60 mT/m gradients. To raise the signal to noise ratio, a commercially available circular surface coil of 23 mm in diameter was used (Micro 23; Philips Medical Systems). Turbo spin echo (TSE) T_2 (time of repetition [TR] 3,595, time of echo [TE] 96, thickness [Thk] 0.75 mm, field of view [FOV] 50), TSE T_1 (TR 600, TE 23, Thk 0.75 mm, FOV 50), and fast field echo T_2* (TR 326, TE 9.21, fractional anisotropy 32°, Thk 0.8 mm, FOV 55) sequences of these agarose phantoms were acquired.

Experimental Autoimmune Encephalomyelitis Induction and NPC Transplantation

Chronic-progressive experimental autoimmune encephalomyelitis (EAE) was induced in 6–8-week-old C57BL/6 female mice as described [18, 20]. Further information is provided in the supplemental online Methods.

In Vivo MR Imaging

In vivo studies were performed on a 3 Tesla (3T) human MR scanner (Intera 3T; Philips Medical Systems) equipped with 40 mT/m gradients. A compatible mouse-brain dedicated commercially available quadrature surface coil (RAPID Biomedical, Rimpar, Germany, http://www.rapidbiomed.de) was used. At due time points, EAE mice were imaged under general gas anesthesia (5% Sevoflurane [Sevorane; Abbott Laboratories, Abbott Park, IL, http://www.abbott.com] for anesthesia induction followed by 1%–2% Sevoflurane for anesthesia maintenance, both in a mixture of 95%–99% O_2). During the entire acquisition time, mice were positioned prone on a MR-compatible temperature control unit (RAPID Biomedical). Further information and MR sequence parameters are provided in the supplemental online Methods.

Relaxometry

In vitro and ex vivo relaxometry studies were performed on a 1.5 Tesla human MR scanner equipped with a circular surface coil of 23 mm in diameter. To obtain T_2 relaxometry (R2), a spin echo-multiecho sequence (TR 2,500) with eight echo times ranging between 50 and 400 milliseconds (ms) was acquired, and reconstructions of T_2 maps were obtained by interpolating the signal curve for the different echo times. R2 rate was then calculated as $1/T_2$. T_2* relaxometry was obtained using multishot echo planar imaging (EPI) sequence with removed blip gradients to apply the same phase-encoding to all gradient echoes. A series of images at different echo times from one EPI train was then reconstructed. Complex data were collected to calculate the phase distribution for B0 maps to correct for macroscopic delta B0 influences. A multislice approach was used for the EPI sequence (TR 200 ms, delta-TE 3.3 ms, voxel size 0.4 × 0.4 × 0.8 mm for liver and spleen and 0.1 × 0.1 × 0.5 for brain) as previously described [16]. Further information is provided in the supplemental online Methods.

Histology

At due time points, mice to sacrifice ($n = 4–6$ per time point) were perfused with 4% paraformaldehyde, and brains were removed and either embedded in paraffin or frozen, as previously described [17, 18]. Further information is provided in the supplemental online Methods.

Statistical Analysis

An unpaired Student's t test was used to compare viability and multipotentiality of labeled and unlabeled NPCs. Serial monitoring of (a) meningeal gadolinium enhancement, (b) number of T_1 post-gadolinium enhancing MR lesions, and (c) number of T_2 MR hyperintense lesions in EAE mice were analyzed by one-way analysis of variance followed by Newman-Keuls test. The same test was used for the statistical analysis of R2* values of regions of interest (ROIs) of organs from transplanted and control mice. Statistical

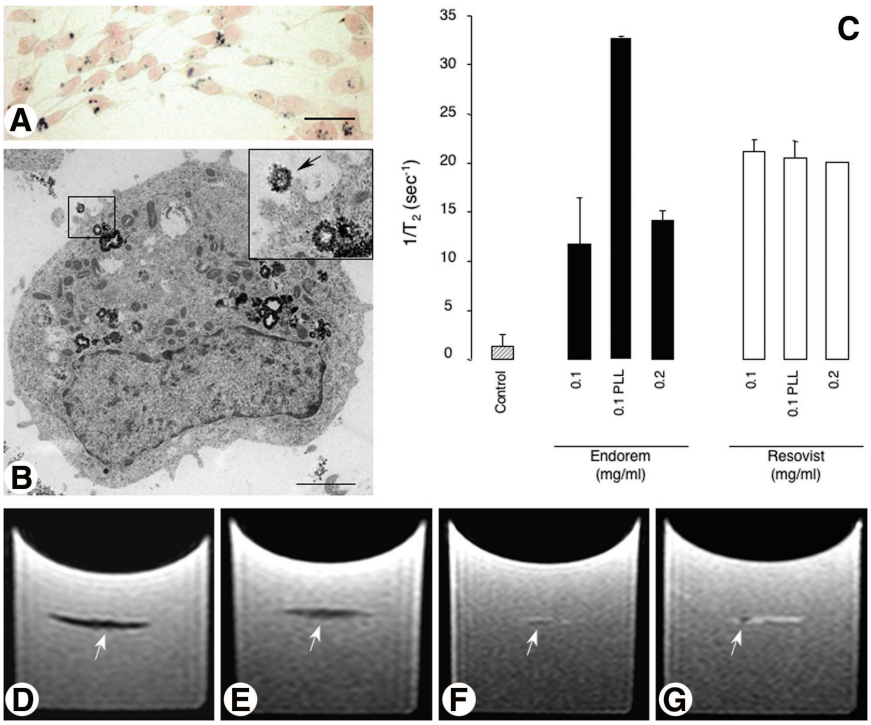

Figure 1. Labeling of neural stem/precursor cells (NPCs) with superparamagnetic iron-oxide (SPIO) particles. **(A):** Perl's Prussian blue staining of matrigel-adhered NPCs. Nuclei are counterstained with nuclear red, whereas SPIO particles are stained in dark blue. Scale bar = 20 μm. **(B):** Electron microscopic in vitro appearance of a single NPC labeled with 0.1 mg/ml Resovist in vitro. Note the electron-dense intracytoplasmic SPIO inclusions within the cell. The inset shows two electron dense aggregates, one of which is still extracellular (arrow), and it is being included by invagination of the cell membrane leading to endocytosis. Scale bar = 2 μm. **(C):** Magnetic resonance (MR)-based relaxometry of NPCs incorporating Endorem (black bars) and Resovist (white bars) at 0.1–0.2 mg/ml iron in the presence or absence of PLL. Wide upward diagonal bars represent nonlabeled control NPCs. **(D–G):** MR T_2-weighted images of gelatin blocks containing focally seeded 10^4 **(D)**, 10^3 **(E)**, 10^2 **(F)**, and 10 **(G)** NPCs labeled with Resovist. Arrows indicate dark (hypointense) areas containing labeled cells. Abbreviations: PLL, poly-L-lysine; sec^{-1}, $seconds^{-1}$.

significance was accepted with a p value $\leq$ .05. Coefficient of determination (r^2) was calculated with linear regression analysis to characterize the relationships among R2* rate per number of cells per ROI in relaxometry studies.

RESULTS

Labeling of Adult NPCs with FDA-Approved Superparamagnetic Iron-Oxide Particles

Initially, we set out to identify the ideal protocol for magnetic labeling of NPCs using superparamagnetic iron-oxide particles. Cell labeling was carried out by either direct exposure of the cells to the SPIOs or by complexing the SPIOs to a polycationic transfection reagent [21].

To determine the ideal contrast agent, we first evaluated the MR properties of three dextran-coated iron-oxide human-grade MR contrast agents, namely Endorem, Resovist, and Sinerem. To improve cell uptake of the contrast agents, we also evaluated the utility of preconjugating the SPIOs with the transfecting agent poly-L-lysine (PLL) [22]. T_2 MR relaxometry ($R2 = 1/T_2$) allows precise quantification of the MR signal induced by iron-based contrast media [23]. To set the ideal SPIO/PLL ratio for each of the three contrast agents tested, we first performed MR-based relaxometry at a fixed iron concentration (100 nM) of the three SPIOs complexed to PLL at different SPIO/PLL ratios. The most efficient signal change, as demonstrated by increase of the R2 values, was obtained at a 1:0.01 SPIO/PLL ratio for Resovist and Sinerem and at 1:0.03 for Endorem (supplemental online Fig. 1).

Next, NPCs were incubated for 72 hours in vitro with different concentrations of Endorem, Resovist, and Sinerem either alone or complexed with PLL. At an iron concentration $\geq$0.2 mg/ml, we observed significant accumulation of extracellular iron precipitates by Perl's PB staining for all the SPIOs tested (data not shown) whether PLL-conjugated or not. Since these extracellular precipitates might be unfavorable to accurate MR imaging, we performed cell labeling with lower concentrations of SPIOs. Indeed, by incubating cells with 0.1 mg/ml iron, we could achieve 97.6%, 100%, and 15.4% NPC labeling efficiency with Endorem, Resovist, and Sinerem, respectively, as determined by PB staining. Furthermore, at this concentration, distinctive blue cytoplasmic inclusions were only detected in cells incubated with SPIOs (Fig. 1A). Thus, this labeling protocol enhanced signal specificity while preserving labeling efficiency of NPCs.

The electron microscopic appearance of SPIO-labeled NPCs revealed multiple dark electron-dense cytoplasmic inclusions (Fig. 1B, supplemental online Fig. 2), which at high power appeared granular (Fig. 1B, inset) and surrounded by a membrane (supplemental online Fig. 2), a feature suggestive of either endo- or pinocytosis, as previously described [13, 24]. These cytoplasmic inclusions were never seen in unlabeled control cells (data not shown). This appearance was similar to that previously reported after SPIO labeling of other neural cell types, such as oligodendrocyte progenitors [9] or Schwann cells [13].

In order to better determine differences in absolute cellular iron incorporation between Endorem and Resovist, we carried out MR relaxometry-based iron quantification on labeled NPCs. NPCs incubated with 0.1 mg/ml Endorem/PLL complexes showed the best relaxation properties (32.7 $\pm$ 4.7 $seconds^{-1}$) when compared with the very same contrast agent at 0.1 and 0.2 mg/ml iron in the absence of PLL. Incubation of NPCs with Resovist—at any condition tested—showed intermediate, although more reliable, relaxation performances. Indeed, there was no difference in absolute cellular iron incorporation between 0.1 and 0.2 mg/ml iron (21.20 $\pm$ 1.1 $seconds^{-1}$ and 20.1 $\pm$ 0.02 $seconds^{-1}$, respectively) with or without PLL (Fig. 1C). Furthermore, cell viability was not affected by incubation of NPCs with Resovist (mean cell viability: 88% $\pm$ 1%) when compared with control NPCs (mean cell viability: 85% $\pm$ 1%). Thus, these studies indicated that optimal NPC labeling is reached with Resovist.

To further validate our labeling protocol, the Resovist-labeled NPCs were placed in agarose phantoms and subjected to

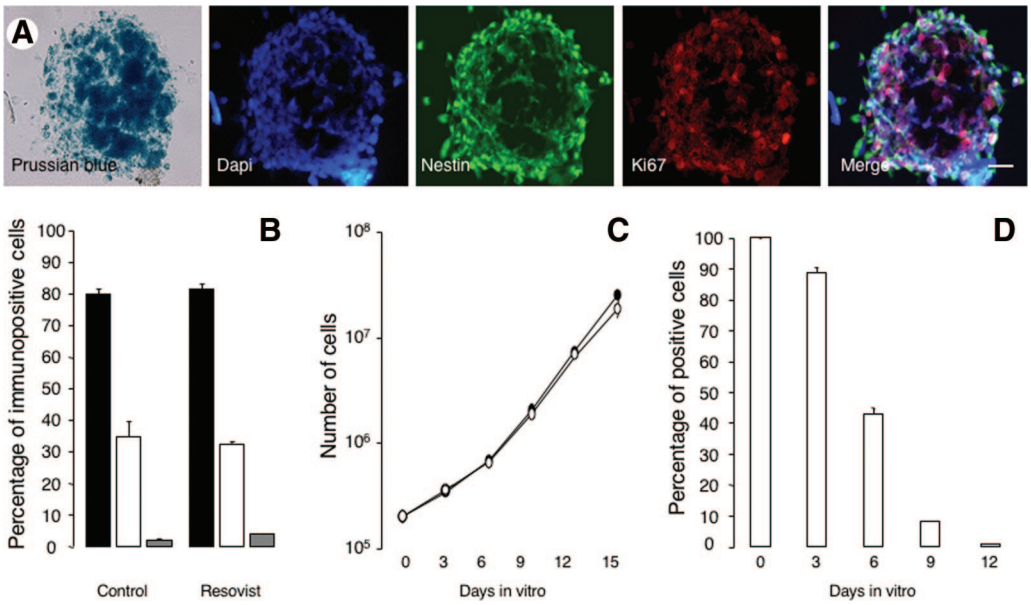

Figure 2. Labeling with Resovist does not interfere with major biological properties of adult neural stem/precursor cells (NPCs). **(A):** Prussian blue (PB) phase micrograph and fluorescence images of a representative neurosphere, as NPCs appear after culturing single dissociated NPCs together with 0.1 mg/ml Resovist for 72 hours in vitro. Nuclei are counterstained with nuclear red, whereas superparamagnetic iron-oxide particles are stained in dark blue. Scale bar = 50 μm. **(B):** In vitro multipotency upon growth factor (GF) withdrawal is retained by Resovist-labeled NPCs, as shown by quantification of astrocytes (glial fibrillary acidic protein, black bars), neurons (β-tubulin-III, white bars), and oligodendrocytes (galactocerebroside, gray bars). **(C):** In vitro self-renewal in GF-enriched culture medium is retained by Resovist-labeled NPCs, as shown by continuous growth curves displaying steady expansion rates in control NPCs (black circles) and NPCs labeled with Resovist (white circles). **(D):** Continuous growth of Resovist-loaded NPCs for a total of five passages of amplification in vitro shows progressive fading of the percentage of PB-positive cells over passaging. Abbreviation: Dapi, 4,6-diamidino-2-phenylindole.

MR T_2- and T_2*-weighted imaging. Visualization of down to 10 Resovist-labeled NPCs was achieved and, as expected, Resovist-labeled NPCs appeared as small dark (hypointense) areas (Fig. 1D–1G, arrows). NPCs labeling with Resovist/PLL complexes did not improve the detection limit (data not shown).

Furthermore, labeling of NPCs with Resovist did not affect expression of major antigens of immature neural cells (such as nestin) within spheres or markers of cell cycle entry such as Ki67 (Fig. 2A). In vitro multipotentiality upon growth factor withdrawal was not affected, either (Fig. 2B). Finally, NPCs labeled with Resovist displayed steady expansion rates (Fig. 2C), which were comparable with those of nonlabeled control cells. However, during 12-day expansion, we observed a progressive decrease in the percentage of iron-positive cells, thus indicating that the majority of iron loss may occur during cell proliferation (Fig. 2D), as previously suggested [15, 25].

Monitoring Disease Onset and Progression in the Myelin Oligodendrocyte Glycoprotein-35–55-Induced EAE by Sequential Clinical-Graded MR Imaging

We next set out to assess the feasibility of monitoring disease onset and progression by clinical-grade MR in mice affected by chronic EAE by comparing brain lesions at different stages—defined by histopathology—with MR imaging. C57BL/6 mice were immunized with myelin oligodendrocyte glycoprotein (MOG)35–55, as described [18], and subjected to in vivo MR imaging at different time points postimmunization (days postimmunization [dpi]).

The gain of gadolinium enhancement in T_1 MR images measures the disruption of local endothelial barriers, and it is routinely used in humans as a surrogate marker of CNS cellular infiltration [26]. In T_1 postgadolinium MR images, we observed diffuse pial and/or meningeal enhancement, which started appearing as early as 7 dpi in 85.7% of immunized mice (Fig. 3A). Therefore, in our experimental setting, this finding could be suggestive of preclinical meningitis [27, 28]. As a matter of fact, by 11–15 dpi, 100% of mice had peak diffuse meningeal enhancement in T_1 postgadolinium MR images (Fig. 3B). This enhancement progressively faded at later time points, so that, as late as 32 dpi, EAE mice still showed a very faint meningeal postgadolinium enhancement ($p \leq .005$ when compared with 15 dpi) (Fig. 3J). Histopathological analysis at clinical disease onset (e.g., 15 dpi) confirmed the presence of numerous $CD3^+$ blood-borne inflammatory cells diffusely infiltrating the submeningeal space(s) and forming perivascular cuffs around brain leptomeningeal vessels (Fig. 3C).

We then carried out T_2 MR imaging. This is done to study the occurrence of increased water content within the CNS parenchyma, which, in EAE/MS, may reflect the presence of focal areas of inflammatory edema, demyelination, astrogliosis, axonal damage, or subtle blood-brain barrier disturbance not detected with gadolinium [29].

Using this approach, we found several bright (hyperintense) brain parenchymal lesions, which were colocalizing with the areas showing gadolinium enhancement in T_1 MR images. These T_2 and T_1 postgadolinium hyperintense inflammatory lesions were first detected in 83% and 85.7% of mice between 7 and 11 dpi, respectively. MR-based detection of T_2 MR hyperintense brain parenchymal lesions peaked at 17 dpi (100% of mice) (Fig. 3D, 3E). The inflammatory significance of these hyperintense brain areas was confirmed by histopathology, which demonstrated large infiltrations of $CD3^+$ blood-borne cells at the lesion sites (Fig. 3F).

Acutely to EAE clinical onset, between 16 and 18 dpi, 92.6% (75/81 scored) of T_2 MR hyperintense brain parenchymal lesions retained gadolinium enhancement, whereas, after the clinical peak of the disease—namely 25 dpi, only 37.5% (6/16 scored) of the above MR identified brain parenchymal lesions showed gadolinium enhancement (55% less,

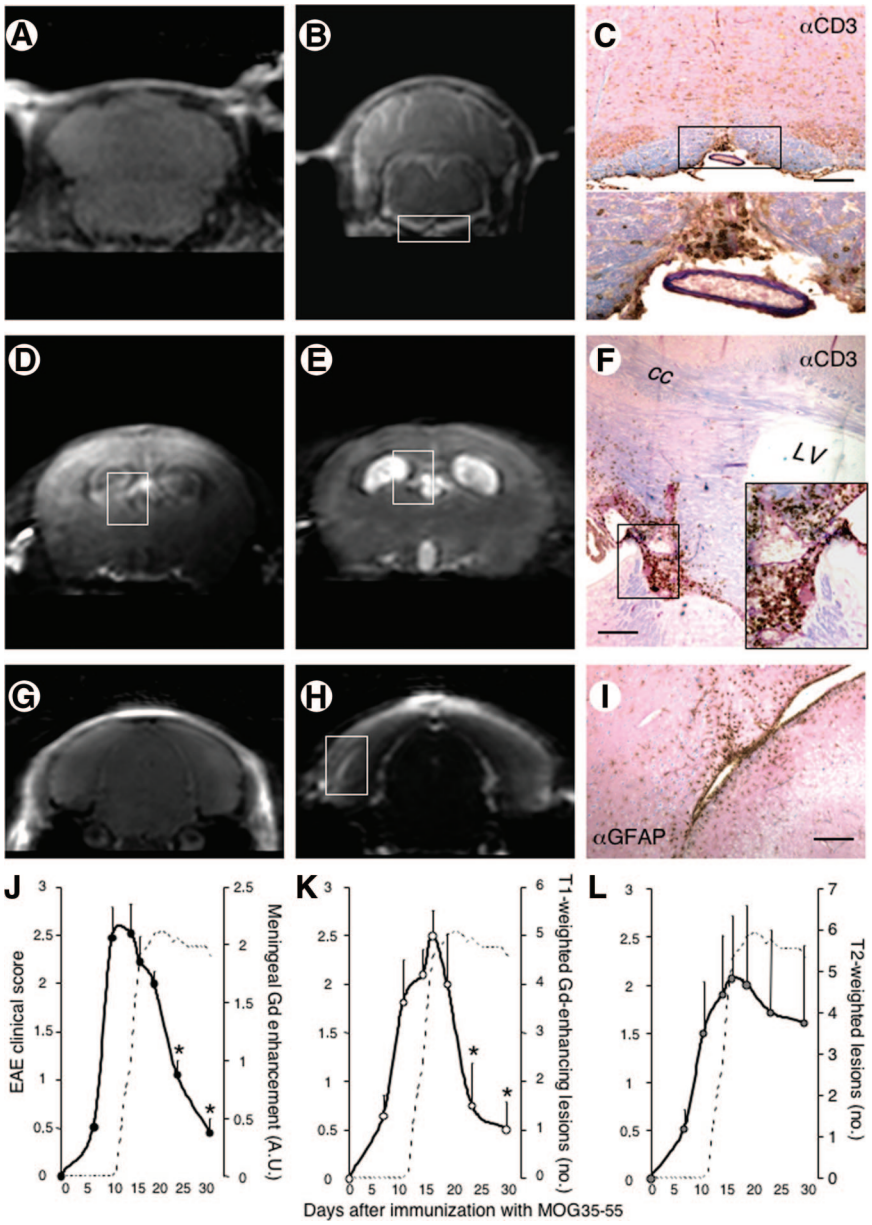

Figure 3. In vivo magnetic resonance (MR) and postmortem pathology correlates of early acute and late chronic features of MOG35–55-induced EAE in mice. **(A):** Representative coronal T_1 postgadolinium MR image at the level of the brainstem and cerebellum of an EAE mouse performed during early preclinical disease phase (i.e., 7 days postimmunization [dpi]). **(B):** Representative coronal T_1 postgadolinium MR image of the very same EAE mouse obtained at the same level shown in **(A)**, performed during early acute disease phase (i.e., 15 dpi). The box highlights the diffuse meningeal gadolinium enhancement. **(C):** Histopathological analysis of the MR-detected lesion as in the box in **(B)**. Luxol fast blue (LFB)-stained brain section showing $CD3^+$ blood-borne cells (brown) diffusely infiltrating the submeningeal space and forming a perivascular cuffing around a brain leptomeningeal vessel (see detail in the magnified inset). Scale bar = 200 μm. **(D, E):** Representative MR brain coronal sections of an EAE mouse performed during early acute disease phase (i.e., 15 dpi). The periventricular T_1 postgadolinium enhancement in **(D)** and T_2 hyperintensity in **(E)** (boxes) are both suggestive of acute inflammatory demyelination. **(F):** Histopathological analysis of the MR-detected demyelinating lesion as in **(D, E)**. LFB-stained brain section showing $CD3^+$ blood-borne cells (brown) diffusely infiltrating the periventricular white matter (see detail in the magnified inset). Note the pale blue staining of the corpus callosum, suggestive of demyelination. Scale bar = 200 μm. **(G, H):** Representative MR brain coronal images of an EAE mouse performed during late chronic disease phase (i.e., 32 dpi). **(G):** Absence of gadolinium enhancement in the T_1 MR image. **(H):** White matter T_2 MR hyperintensity of the right external capsule (box) is suggestive of chronic white matter abnormality. **(I):** Histopathological analysis of the MR-detected lesion as in **(H)**. LFB-stained brain section showing presence of numerous $GFAP^+$ reactive astrocytes (brown). Scale bar = 200 μm. **(J):** Sequential monitoring of meningeal gadolinium enhancement in EAE by longitudinal in vivo brain MR imaging. **(K, L):** Temporal profiling of the number of T_1 postgadolinium **(K)** and T_2 MR hyperintense **(L)** parenchymal lesions accumulating in the brain of EAE mice at different time points after immunization. Left ordinates in **(J–L)** are referred to the EAE neurological score (dashed line). Data in **(J–L)** are expressed as mean numbers per mice ± SEM; ∗, $p \leq .05$ when compared with 17 dpi. Abbreviations: A.U., arbitrary units; CC, corpus callosum; EAE, experimental autoimmune encephalomyelitis; Gd, gadolinium; GFAP, glial fibrillary acidic protein; LV, lateral ventricle; MOG, myelin oligodendrocyte glycoprotein; no., number.

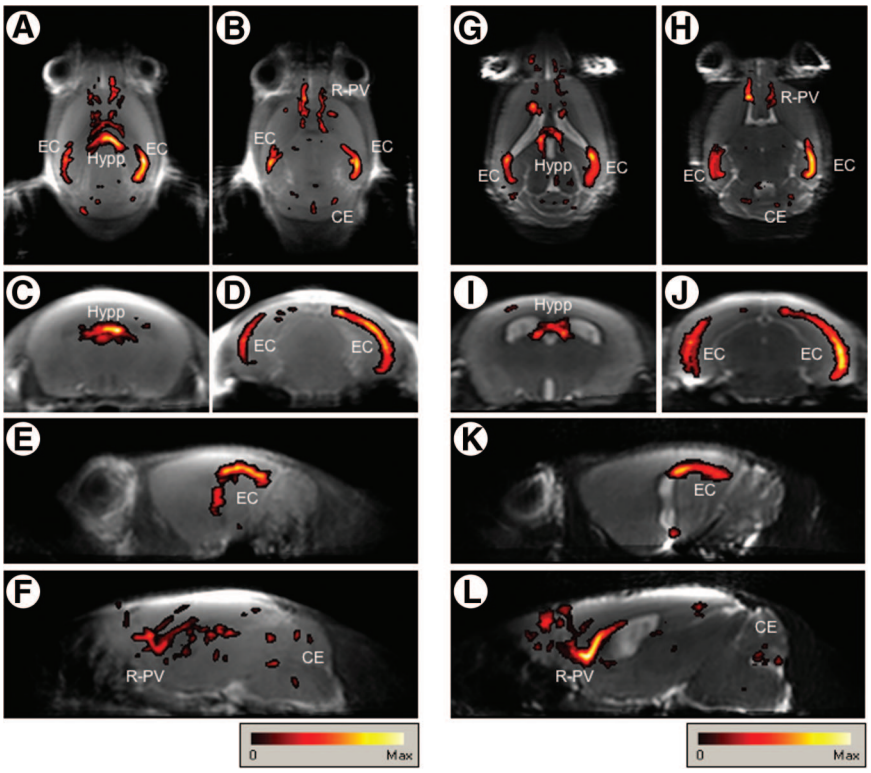

Figure 4. Spatial lesion probability maps of T_1 postgadolinium and T_2 hyperintense brain lesions during the acute phase of myelin oligodendrocyte glycoprotein-35–55-induced experimental autoimmune encephalomyelitis (EAE) in mice. These maps provide a quantitative description of the topographic distribution of lesions across the tested EAE population and are representative of the lesion burden in $n \geq 12$ EAE mice at clinical peak of the disease (e.g., 17 days postimmunization). **(A–F):** T_1 postgadolinium hyperintense lesion probability map. **(G–L):** T_2 hyperintense probability map. Note the overall lesion accumulation with prominent clustering within the rostral-periventricular areas, the external capsule, the hippocampal fimbria, and cerebellum in both maps. **(A, B, G, H):** Axial views. **(C, D, I, J):** Coronal views. **(E, F, K, L):** Sagittal views. The scale bars indicate the probability of lesion per site, ranging from 0% (transparent) to 100% (yellow). Abbreviations: CE, cerebellum; EC, external capsule; Hypp, hippocampal fimbria; Max, maximum; R-PV, rostral-periventricular.

$p \leq .05$). This suggests a progressive fading of the inflammatory component(s) within the brain.

Within a more chronic disease phase, namely 32 dpi, a further 30% decrease of the number of inflammatory T_2 MR hyperintense brain lesions (4/15, 26%) was also observed. In each lesion, gadolinium enhancement was detectable for approximately 7 ($\pm$3) days.

The total number of T_2 MR hyperintense brain lesions peaked at 17 dpi but slightly decreased at later time points (Fig. 3L). Histopathology of late (i.e., 32 dpi) inactive T_2 MR hyperintense brain lesions demonstrated the virtual absence of inflammatory infiltrates (data not shown) together with the presence of numerous reactive glial fibrillary acidic protein-positive astrocytes (Fig. 3I) [30].

The overall in vivo monitoring of the whole accumulation of MR-visible brain lesions showed that half of the T_2 MR hyperintense lesions accumulated between the cerebellum (23.8% $\pm$ 3%) and the more rostral-periventricular brain areas (29.5% $\pm$ 3.2%) (supplemental online Fig. 3). By contrast, the analysis of site lesion probability for T_1 postgadolinium MR brain areas showed greater accumulation of focal hyperintensities within both the external capsule (16.25% $\pm$ 2.7%) as well as the hippocampus (17.9% $\pm$ 3.5%), as compared with T_2 MR images (supplemental online Fig. 3).

Finally, spatial lesion probability maps of both T_2 and T_1 postgadolinium hyperintense brain lesions provided quantitative description of the topographic distribution of lesions across the tested EAE population and confirmed the data collected at both histopathology and conventional MR imaging (Fig. 4). These results, altogether, demonstrate that number, time of appearance, and load of T_2 MR hyperintense brain lesions, despite varying greatly among MOG35–55-immunized mice, have an overall similar distribution of the lesion site(s). Furthermore, the appearance and evolution of brain lesions induced in the chronic model of EAE can be studied in detail with clinical-grade MR imaging.

In Vivo MR Imaging of Resovist-Labeled NPCs Injected Intravenously into EAE Mice

To monitor NPC site accumulation in a disease setting, we performed experiments by transplanting green fluorescent protein (GFP)-expressing NPCs labeled with Resovist into MOG35–55-induced chronic EAE C57BL/6 mice. NPCs (10^6 cells per mouse) were injected intravenously at the peak of brain inflammation—namely, 17 dpi—as indicated by postgadolinium enhancement in T_1 MR images, corresponding to the early clinical phase of the disease. EAE mice used for in vivo transplantation studies underwent serial 3T brain MR imaging at 24 hours preinjection (Pre), 24–48 hours postinjection (Post), and 18 days postinjection (Late).

T_2 MR Post focal brain hypointensities (4.16 $\pm$ 0.7 per mouse) were observed as early as 24 hours post-transplantation. All these MR hypointense brain areas had appeared hyperintense in both postgadolinium T_1 and T_2 MR Pre images, whereas none of them was observed in the normal intense brain parenchyma (Fig. 5A–5C). In order to confirm the specific accumulation of transplanted NPCs within MR-visible brain lesions, we carried out postmortem combined PB staining (Fig. 5D, 5E) and GFP/CD45 immunofluorescence analysis on consecutive brain tissue sections (Fig. 5E–5G). PB^+/GFP^+ cells were always negative for CD45 (Fig. 5G), thus suggesting that the visualized MR signal was not due to uptake of the SPIOs by phagocytes.

Half of the T_2 MR Pre hyperintense focal brain lesions turned hypointense at 24–48 hours and 16–18 days after NPC transplantation (52.7% and 54.5%, respectively) (Fig. 5H). Moreover, site-specific analysis of NPC accumulation showed that 80% ($\pm$12.9) of MR-visible brain lesions of the external capsule and 68.18% ($\pm$13.3) of the rostral-periventricular forebrain appeared as favored accumulation site(s) for systemically injected NPCs at MR Post imaging (Fig. 5H). Cell accumulation probability maps confirmed the preferential NPC accumulation at the same sites of both T_1 postgadolinium and T_2 MR Pre images (Fig. 5I–5L). No T_2 MR Post brain hypointensities were

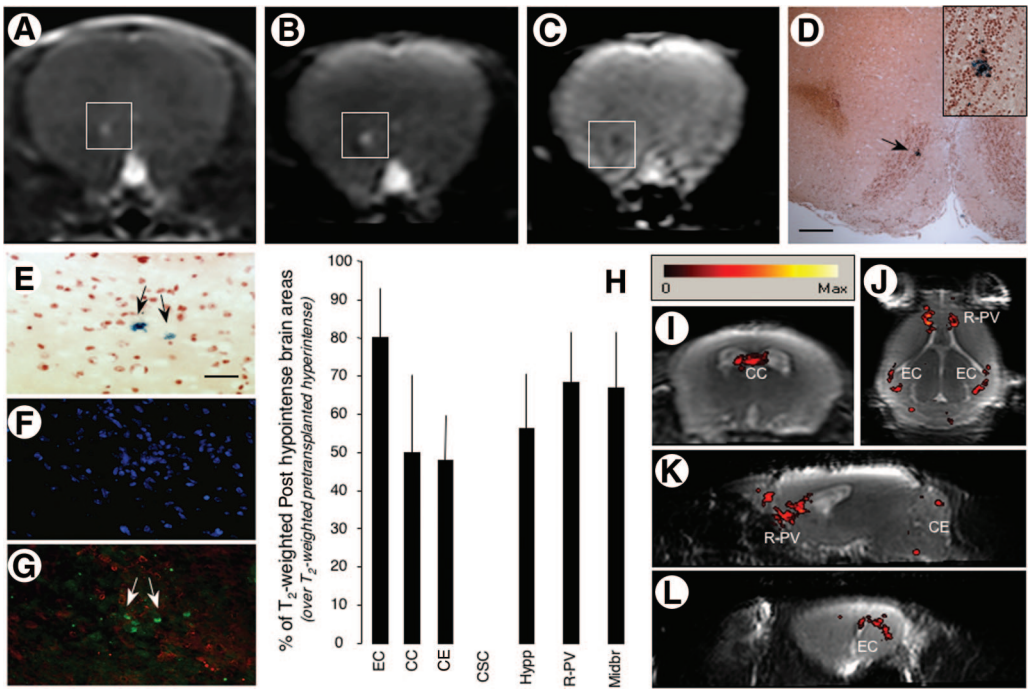

Figure 5. In vivo brain magnetic resonance (MR) images of Resovist-labeled neural stem/precursor cells (NPCs) injected intravenously in experimental autoimmune encephalomyelitis (EAE) mice. **(A–C):** In vivo brain MR images of a representative EAE mouse injected intravenously with Resovist-labeled NPCs. Coronal postcontrast T_1 **(A)** and T_2 **(B)** MR images of the brain at 17 days postimmunization (dpi) showing the presence of a focal T_2 hyperintense lesion in the right frontal pole gaining enhancement after gadolinium infusion (boxes in **[B]** and **[A]**, respectively). **(C):** Coronal T_2 brain MR image of the same mouse obtained at the same level 24 hours (i.e., 18 dpi) after i.v. injection of 10^6 Resovist-labeled NPCs. The box in **(C)** points to focal hypointensity appearing over previously observed hyperintensity in T_2-weighted image, thus suggesting the accumulation of iron-labeled NPCs. **(D):** Prussian blue (PB) staining of a brain coronal section obtained at the same level of MR scans in **(A–C)**, indicating the presence of iron-labeled NPCs (arrow). See detail in the magnified inset. Scale bar = 200 μm. Nuclei are counterstained with nuclear red. **(E–G):** Representative PB **(E)** and double green fluorescent protein (GFP)/CD45 immunofluorescence stainings **(G)** of two consecutive 5 μm-thick brain coronal sections showing the presence of two PB^+/GFP^+ NPCs (arrows in **[E, G]**) not colocalizing with CD45-expressing blood-borne inflammatory cells. GFP is in green, whereas CD45 is in red in **(G)**. Nuclei in **(E)** are counterstained with nuclear red, whereas those in **(F)** are counterstained with 4,6-diamidino-2-phenylindole. Scale bar = 35 μm. **(H):** Site-specific distribution of putative inflammatory demyelinating brain lesions appearing as predictive accumulation site(s) of Resovist-labeled NPCs injected intravenously into EAE mice. **(I–L):** Cell accumulation probability map confirming quantitative prevalence of transplanted NPCs within the very same brain areas as in **(H)**. The map is representative of the accumulation of intravenously injected NPCs in the brain of $n \geq 11$ EAE mice at 24–48 hours after transplantation. **(I):** Coronal view. **(J):** Axial view. **(K, L):** Sagittal views. The scale bar indicates the probability of cells per site, ranging from 0 (transparent) to max (yellow). Abbreviations: CC, corpus callosum; CE, cerebellum; CSC, cortico-subcortical; EC, external capsule; Hypp, hippocampus; Max, maximum; Midbr, midbrain; R-PV, rostral-periventricular.

ever observed in control mice injected intravenously with either Resovist-labeled NPCs or with Resovist only (data not shown). In line with previous evidence, T_2 MR images of peripheral filter organs, such as the liver and the spleen, indicated that, early after transplantation, considerable numbers of transplanted NPCs also accumulate into bodily sites other than the CNS (supplemental online Fig. 4) [18]. These findings suggest that selective (inflammation-specific) accumulation of systemically injected NPCs takes place in more than half of putative inflammatory brain lesions in EAE.

Noninvasive MR-Based Quantification of NPC Accumulation Within the Brain of Transplanted EAE Mice

The possibility of quantifying the biodistribution of transplanted cells and assessing the number of labeled cells accumulating into target tissues is of critical value for the optimization of both dose and timing of cellular therapies in experimental studies as well as human clinical trials. The R2* (1/T2*) relaxation rate is being proposed as a highly sensitive measure allowing precise quantification of MR signal in different areas or across different examinations, and it has previously been validated for quantitative, in vivo detection of intracellular SPIOs [16, 31]. Using a standard calibration curve, quantitative prediction of the number of labeled cells in a given region could be therefore obtained. We decided to use R2*-based noninvasive imaging for determining the number of labeled NPCs accumulating within the brain of EAE mice.

We first calculated the corrected R2* values from post-transplantation T_2 MR hypointense-appearing brain areas (HABA) of EAE mice injected intravenously with Resovist-labeled NPCs. R2* values from post-transplantation HABA were significantly higher than R2* acquired from normal-appearing brain areas (NABA) of both transplanted and control mice ($p \leq .05$) (Fig. 6A). This confirms both the imaging data as well as previous pathological studies [18, 32], indicating selective homing of transplanted NPCs into inflammatory demyelinating brain lesions.

Of note, we did not find any significant difference of R2* HABA values between NPC-transplanted EAE mice sacrificed at either 3 or 18 days post-transplantation (dpt). Again, no differences of R2* values were ever found in NABA from either group of mice, thus providing further unequivocal evidence for specific NPC accumulation within the inflamed CNS following systemic injection [1]. Relaxometry also showed that liver and spleen R2* of all groups of mice injected intravenously with either Resovist-labeled NPCs or Resovist only were significantly higher than R2* from sham-treated mice (Fig. 6B; $p \leq .001$; supplemental online Fig. 4).

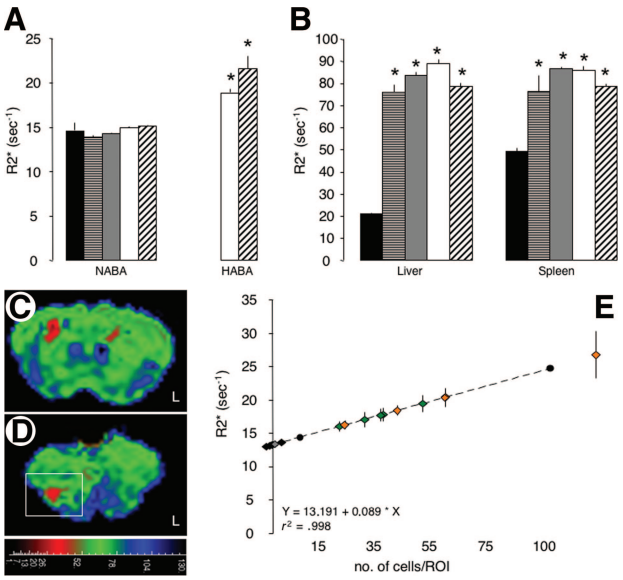

Figure 6. Ex vivo noninvasive R2*-based quantitative prediction of bodily distribution of neural stem/precursor cells (NPCs) injected intravenously. Ex vivo corrected R2* analysis of normal-appearing brain areas, hypointense-appearing brain areas, liver and spleen from sham-treated experimental autoimmune encephalomyelitis (EAE) mice (black), healthy control mice injected intravenously with either Resovist only (narrow horizontal) or with 10^6 Resovist-labeled NPCs (gray), and two different groups of EAE mice injected intravenously with 10^6 Resovist-labeled NPCs sacrificed at either 3 days post-transplantation (dpt) (white) or at 18 dpt (wide upward-diagonal striped). Accumulation of Resovist-labeled NPCs within the brain of EAE mice **(A)**, as well as within liver and spleen of both EAE and healthy control mice **(B)**, significantly lengthened the R2* relaxation times; *, $p \leq .05$ when compared with sham-treated EAE mice. **(C–E):** T_2* relaxometric determination of the quantitative relationship between the numbers of transplanted cells and brain R2* relaxation rate in EAE mice injected intravenously with Resovist-labeled NPCs. **(C, D):** Representative corrected T_2* maps of the brain from a healthy control mouse stereotaxically injected with 10 (left hemisphere) versus 10^2 (right hemisphere) Resovist-labeled NPCs **(C)** or an EAE mouse injected intravenously with 10^6 Resovist-labeled NPCs **(D)**. The box in **(D)** highlights the remarkable variation of R2* pattern within a presumptive site of cell accumulation in the right frontal pole. **(E):** Magnetic resonance-based approximation of the number of labeled NPCs accumulating within brain lesions of transplanted EAE mice. Dashed line represents the function of correlation between R2* values and labeled cells, calculated by linear interpolation of corrected R2* values of calibration brain phantoms injected intraparenchymally with known numbers of labeled NPCs (black dots) ($r^2 = .998$). Spots represent the average of corrected R2* of all T_2-weighted post-transplantation hypointense areas per mouse, whereas SEM bars are indicative of variations within EAE mice transplanted with NPCs. Gray, healthy control mice transplanted with Resovist-labeled NPCs; black, sham-treated EAE mice; green, EAE mice transplanted with NPCs and sacrificed at 3 dpt; orange, EAE mice transplanted with NPCs and sacrificed at 18 dpt. Abbreviations: HABA, hypointense-appearing brain areas; L, left hemisphere; NABA, normal-appearing brain areas; no., number; ROI, region of interest; sec^{-1}, $seconds^{-1}$.

Finally, in order to predict the number of iron oxide-labeled NPCs accumulating within MR-identifiable inflammatory demyelinating brain lesions, we used a reference standard curve obtained by intraparenchymal transplantation of known number of labeled NPCs (see supplemental online Methods for details) and performed simple regression analysis on brain tissue R2* values and number of labeled NPCs per ROI ($r^2 = .998$). Average R2* values of T_2 MR Post hypointense areas from transplanted EAE mice varied between 33.3–74.4 cells per ROI at 3 dpt and between 35.8–164.4 cells per ROI at 18 dpt (Fig. 6C–6E). Overall, these data, collected with a noninvasive MR-based technique, significantly correlated with previous findings from our own and other laboratories investigating the efficiency of homing into the CNS of NPCs injected systemically into EAE mice [17].

DISCUSSION

In CNS disorders characterized by neuronal or glial loss (e.g., stroke, Parkinson disease, MS, spinal cord injury), NPC-based replacement therapies represent a promising alternative therapeutic approach [1]. However, there are some relevant and preliminary issues that need to be addressed before envisaging any potential human application of such therapies: (a) the ideal cell source for transplantation; (b) the route of cell administration, optimal cell doses, and correct therapeutic window; and (c) the differentiation and persistence of transplanted cells into the targeted tissue. Furthermore, functional and long-lasting integration of transplanted cells into the host tissue has to be achieved [33]. To better understand and detail these events and to foresee any human translation of such promising therapies, we would certainly benefit from a reliable noninvasive imaging system able to follow the in vivo fate of transplanted cells. This would be particularly helpful in certain CNS multifocal inflammatory disorders (e.g., MS, stroke, etc.) in which systemically (e.g., intravenously, intrathecally) transplanted NPCs accumulate (and persist) within inflammatory lesions throughout the whole CNS [17, 18, 32]. The latter is due to the demonstrated ability of NPCs to follow, via the blood stream or cerebrospinal fluid circulation, a gradient of certain chemoattractants (e.g., proinflammatory cytokines and chemokines) occurring at the site of inflammatory CNS lesions [17, 18, 32, 34]. To specifically address the issue of whether systemically injected somatic stem cells might be sensitively monitored in vivo upon transplantation, we used as a model system a multifocal CNS-confined inflammatory demyelinating experimental disease such as EAE.

Among all available imaging techniques, MR imaging presents several advantages, since it offers both near-cellular (i.e., 25–50 μm) resolution and whole-body imaging capability along with excellent soft tissue contrast [7]. The usefulness of MR imaging mainly relies on its high spatial resolution and direct anatomical correlation, which allows relatively precise localization of labeled cells. MR imaging—and in particular T_2-weighted imaging—permits direct in vivo colocalization of cells within demyelinating lesions, thus being sensitive enough for demonstration of correct NPC engraftment into multiple brain lesions in EAE/MS. Furthermore, MR imaging is commonly used in clinical practice, particularly for studying human CNS, and represents the gold standard examination for diagnosis and monitoring of patients suffering from MS.

We first developed a reliable labeling protocol for NPCs using SPIOs either complexed or not with a polycationic transfecting agent (i.e., PLL) [21]. Properties of three different human-grade SPIOs (two of which are FDA-approved [Endorem and Resovist] and one having completed phase III-B [Sinerem]) were compared in vitro. T_2 relaxometry allowed us reliable comparison of intracellular iron content between different labeling protocols. Among the tested SPIOs, Resovist turned out to be the most sensitive and reliable contrast agent—even in the absence of PLL—and it did not affect major biological properties of NPCs, such as undifferentiation, capacity of self-renewal, and multipotency. These latter findings support previous studies demonstrating the biological inertness of other SPIOs on neural versus non-neural cell types [6, 9, 13]. Therefore, this efficient NPC labeling with Resovist—without requiring additional use of

not yet clinically applicable transfecting agents—prompted us to measure the labeling efficiency of this contrast agent also in vivo.

We then assessed feasibility and sensitivity of monitoring the natural history of mouse chronic EAE by sequential clinical-grade in vivo MR imaging. MOG-immunized EAE mice were serially scanned either at preclinical (7–11 dpi), early acute clinical (15–18 dpi), or late chronic clinical (20–32 dpi) phase(s). Good correlation between in vivo MR images and postmortem neuropathology was found. We visualized both (sub)meningeal inflammation preceding the clinical disease onset as well as inflammatory perivascular infiltrates, mainly composed by blood-borne inflammatory mononuclear cells, leading to the appearance of several brain focal inflammatory and/or demyelinating areas (e.g., cerebellum, rostral-periventricular forebrain, etc.). Furthermore, by MR monitoring, we defined a common lesion distribution pattern in immunized mice. Therefore, sequential clinical-grade in vivo MR imaging appeared as a sensitive noninvasive tool for monitoring disease evolution in small rodents with experimental MS [35–37].

Resovist-labeled NPCs were then injected into the blood streams of mice with clinically established EAE, which were scanned serially for up to 3 weeks post-transplantation. We purposely used this model of multifocal CNS-confined inflammatory demyelination as well as the i.v. cell transplantation protocol in order to check for both feasibility and sensitivity of clinical-grade MR imaging. We know from previous experiments from our own lab [17] that approximately 1%–3% of intravenously injected NPCs accumulate within the brain of EAE mice, thus implying that only a few hundred injected cells might accumulate into single demyelinating inflammatory lesions. In this study, Resovist-labeled NPCs were injected intravenously in EAE mice at the peak of T_1 postgadolinium MR parenchymal enhancement, and accumulation of transplanted cells took place in a significantly high percentage (54.5%) of focal brain areas displaying both neuroradiological and neuropathological features of inflammatory demyelination. Interestingly, the external capsule and the rostral-periventricular forebrain emerged as primary areas of accumulation for intravenously injected NPCs. On the other hand, labeled NPCs were never detected in any of the T_2 MR hyperintense lesions not gaining postcontrast enhancement. It would be interesting to understand, although this is out of the scope of the present work, which would be the pathological features of the subpopulation of MR-identifiable inflammatory demyelinating brain parenchymal lesions into which injected NPCs do (or do not) accumulate. The discrepancy between the number of MR-identifiable inflammatory demyelinating brain parenchymal lesions and that of sites showing accumulation of injected NPCs might be dependent on the asynchronous appearance and/or evolution as well as the pathological heterogeneity of single inflammatory demyelinating lesions in EAE/MS, as previously described [38, 39]. However, we cannot exclude that, in some cases, the clinical-grade apparatus we have been using for these studies may show certain detection limits at the cellular/subcellular level. Our study represents a significant step forward when compared with previously reported approaches on cellular imaging in CNS disorders [13, 40], where intraparenchymal transplantation of known numbers of SPIO-labeled neural cells was performed in a single CNS area, thus not taking into account the in vivo noninvasive quantification of transplanted cells.

To further confirm our results and to estimate the number (detection threshold) of MR-visible SPIO-labeled cells, we also used R2* ($1/T_2$*), corrected for balancing the overestimation of the R2* relaxation rate due to large-scale field inhomogeneities [16]. Several recent studies have demonstrated a high degree of correlation between the tissue iron concentration and corrected R2* values, measured by MR both in vivo and in vitro. Brain tissue corrected R2* values showed that the numbers of iron oxide-labeled NPCs accumulating within inflammatory demyelinating brain lesions ranged between 33.3 and 164.4 cells per site, depending on the timing of MR analysis after cell transplantation. These latter data indicate that the MR protocol we established is sensitive enough to detect in the short time upon cell injection (even) low numbers of transplanted stem cells in the CNS and support previous findings, from our own and other laboratories, investigating homing efficiency into inflamed CNS of NPCs injected systemically into EAE mice [17]. However, we cannot exclude that the noninvasive protocol for in vivo NPC tracking here validated might lose a certain grade of sensitivity and specificity when applied to later time points.

Conclusion

Our study demonstrates at different levels, both in vitro and in vivo, the feasibility of noninvasive clinical-grade MR cellular imaging to monitor and quantify the homing of SPIO-labeled NPCs upon systemic injection into mice affected by a multifocal inflammatory CNS disorder such as EAE. In our view, this represents a significant step toward the design of future clinical trials for somatic stem cell transplantation in MS and other (inflammatory) CNS diseases.

Acknowledgments

We thank Nicoletta Anzalone, Brian D. Brown, and Lawrence Wrabetz for critically discussing and revising the manuscript. We acknowledge the technical help of Susana Amuchastegui, Antonella Iadanza, Carla Panzeri, and Lucia Zanotti. This work was supported in part by the Italian Minister of Health, the Italian Multiple Sclerosis Foundation (FISM; Grant 2004/R/15 to S.P.), the National Multiple Sclerosis Society (NMSS; Grants RG3591-A-1 and TR 3762-A-1 to G.M.), and Fondazione Cariplo "bando chiuso 2005" to G.S. L.S.P. and M.B. contributed equally to this work.

Disclosure of Potential Conflicts of Interest

The authors indicate no potential conflicts of interest.

References

1 Martino G, Pluchino S. The therapeutic potential of neural stem cells. Nat Rev Neurosci 2006;7:395–406.
2 Mendez I, Sanchez-Pernaute R, Cooper O et al. Cell type analysis of functional fetal dopamine cell suspension transplants in the striatum and substantia nigra of patients with Parkinson's disease. Brain 2005;128:1498–1510.
3 Brooks DJ. Positron emission tomography and single-photon emission computed tomography in central nervous system drug development. NeuroRx 2005;2:226–236.
4 Kim DE, Schellingerhout D, Ishii K et al. Imaging of stem cell recruitment to ischemic infarcts in a murine model. Stroke 2004;35:952–957.
5 Jacobs RE, Cherry SR. Complementary emerging techniques: High-resolution PET and MRI. Curr Opin Neurobiol 2001;11:621–629.
6 de Vries IJ, Lesterhuis WJ, Barentsz JO et al. Magnetic resonance tracking of dendritic cells in melanoma patients for monitoring of cellular therapy. Nat Biotechnol 2005;23:1407–1413.

7 Bulte JW, Kraitchman DL. Iron oxide MR contrast agents for molecular and cellular imaging. NMR Biomed 2004;17:484–499.
8 Modo M, Hoehn M, Bulte JW. Cellular MR imaging. Mol Imaging 2005;4:143–164.
9 Franklin RJ, Blaschuk KL, Bearchell MC et al. Magnetic resonance imaging of transplanted oligodendrocyte precursors in the rat brain. Neuroreport 1999;10:3961–3965.
10 Bulte JW, Zhang S, van Gelderen P et al. Neurotransplantation of magnetically labeled oligodendrocyte progenitors: Magnetic resonance tracking of cell migration and myelination. Proc Natl Acad Sci U S A 1999;96:15256–15261.
11 Bulte JW, Douglas T, Witwer B et al. Magnetodendrimers allow endosomal magnetic labeling and in vivo tracking of stem cells. Nat Biotechnol 2001;19:1141–1147.
12 Ben-Hur T, van Heeswijk RB, Einstein O et al. Serial in vivo MR tracking of magnetically labeled neural spheres transplanted in chronic EAE mice. Magn Reson Med 2007;57:164–171.
13 Dunning MD, Lakatos A, Loizou L et al. Superparamagnetic iron oxide-labeled Schwann cells and olfactory ensheathing cells can be traced in vivo by magnetic resonance imaging and retain functional properties after transplantation into the CNS. J Neurosci 2004;24:9799–9810.
14 Daldrup-Link HE, Rudelius M, Piontek G et al. Migration of iron oxide-labeled human hematopoietic progenitor cells in a mouse model: In vivo monitoring with 1.5-T MR imaging equipment. Radiology 2005; 234:197–205.
15 Bos C, Delmas Y, Desmouliere A et al. In vivo MR imaging of intravascularly injected magnetically labeled mesenchymal stem cells in rat kidney and liver. Radiology 2004;233:781–789.
16 Dahnke H, Schaeffter T. Limits of detection of SPIO at 3.0 T using T2 relaxometry. Magn Reson Med 2005;53:1202–1206.
17 Pluchino S, Zanotti L, Rossi B et al. Neurosphere-derived multipotent precursors promote neuroprotection by an immunomodulatory mechanism. Nature 2005;436:266–271.
18 Pluchino S, Quattrini A, Brambilla E et al. Injection of adult neurospheres induces recovery in a chronic model of multiple sclerosis. Nature 2003;422:688–694.
19 Sigal R, Vogl T, Casselman J et al. Lymph node metastases from head and neck squamous cell carcinoma: MR imaging with ultrasmall superparamagnetic iron oxide particles (Sinerem MR)—results of a phase-III multicenter clinical trial. Eur Radiol 2002;12:1104–1113.
20 Amadio S, Pluchino S, Brini E et al. Motor evoked potentials in a mouse model of chronic multiple sclerosis. Muscle Nerve 2006;33:265–273.
21 Arbab AS, Bashaw LA, Miller BR et al. Characterization of biophysical and metabolic properties of cells labeled with superparamagnetic iron oxide nanoparticles and transfection agent for cellular MR imaging. Radiology 2003;229:838–846.
22 Frank JA, Miller BR, Arbab AS et al. Clinically applicable labeling of mammalian and stem cells by combining superparamagnetic iron oxides and transfection agents. Radiology 2003;228:480–487.
23 Koenig SH, Brown RD, 3rd. Relaxometry of magnetic resonance imaging contrast agents. Magn Reson Annu 1987;263–286.
24 Arbab AS, Wilson LB, Ashari P et al. A model of lysosomal metabolism of dextran coated superparamagnetic iron oxide (SPIO) nanoparticles: Implications for cellular magnetic resonance imaging. NMR Biomed 2005;18:383–389.
25 Arbab AS, Bashaw LA, Miller BR et al. Intracytoplasmic tagging of cells with ferumoxides and transfection agent for cellular magnetic resonance imaging after cell transplantation: Methods and techniques. Transplantation 2003;76:1123–1130.
26 Runge VM, Carollo BR, Wolf CR et al. Gd DTPA: A review of clinical indications in central nervous system magnetic resonance imaging. Radiographics 1989;9:929–958.
27 Brown DA, Sawchenko PE. Time course and distribution of inflammatory and neurodegenerative events suggest structural bases for the pathogenesis of experimental autoimmune encephalomyelitis. J Comp Neurol 2007;502:236–260.
28 Chang KH, Han MH, Roh JK et al. Gd-DTPA-enhanced MR imaging of the brain in patients with meningitis: Comparison with CT. AJNR Am J Neuroradiol 1990;11:69–76.
29 Ormerod IE, Miller DH, McDonald WI et al. The role of NMR imaging in the assessment of multiple sclerosis and isolated neurological lesions. A quantitative study. Brain 1987;110:1579–1616.
30 Lassmann H, Bruck W, Lucchinetti C. Heterogeneity of multiple sclerosis pathogenesis: Implications for diagnosis and therapy. Trends Mol Med 2001;7:115–121.
31 Yablonskiy DA, Haacke EM. Theory of NMR signal behavior in magnetically inhomogeneous tissues: The static dephasing regime. Magn Reson Med 1994;32:749–763.
32 Ben-Hur T, Einstein O, Mizrachi-Kol R et al. Transplanted multipotential neural precursor cells migrate into the inflamed white matter in response to experimental autoimmune encephalomyelitis. Glia 2003;41: 73–80.
33 Pluchino S, Furlan R, Martino G. Cell-based remyelinating therapies in multiple sclerosis: Evidence from experimental studies. Curr Opin Neurol 2004;17:247–255.
34 Ransohoff RM. The chemokine system in neuroinflammation: An update. J Infect Dis 2002;186(suppl 2):S152–S156.
35 Rausch M, Hiestand P, Baumann D et al. MRI-based monitoring of inflammation and tissue damage in acute and chronic relapsing EAE. Magn Reson Med 2003;50:309–314.
36 Anderson SA, Shukaliak-Quandt J, Jordan EK et al. Magnetic resonance imaging of labeled T-cells in a mouse model of multiple sclerosis. Ann Neurol 2004;55:654–659.
37 Stoll G, Wesemeier C, Gold R et al. In vivo monitoring of macrophage infiltration in experimental autoimmune neuritis by magnetic resonance imaging. J Neuroimmunol 2004;149:142–146.
38 Morrissey SP, Stodal H, Zettl U et al. In vivo MRI and its histological correlates in acute adoptive transfer experimental allergic encephalomyelitis. Quantification of inflammation and oedema. Brain 1996;119: 239–248.
39 Lucchinetti CF, Bruck W, Rodriguez M et al. Distinct patterns of multiple sclerosis pathology indicates heterogeneity on pathogenesis. Brain Pathol 1996;6:259–274.
40 Bulte JW, Ben-Hur T, Miller BR et al. MR microscopy of magnetically labeled neurospheres transplanted into the Lewis EAE rat brain. Magn Reson Med 2003;50:201–205.

See www.StemCells.com for supplemental material available online.

Magnetic Resonance-Based Tracking and Quantification of Intravenously Injected Neural Stem Cell Accumulation in the Brains of Mice with Experimental Multiple Sclerosis

Letterio S. Politi, Marco Bacigaluppi, Elena Brambilla, Marcello Cadioli, Andrea Falini, Giancarlo Comi, Giuseppe Scotti, Gianvito Martino and Stefano Pluchino

Stem Cells 2007;25;2583-2592; originally published online Jun 28, 2007;
DOI: 10.1634/stemcells.2007-0037